42nd AIAA Aerospace Sciences Meeting and Exhibit
5 - 8 January 2004, Reno, Nevada

AIAA 2004-1095

Airfoil Shape Optimization Using NURBS Representation Under Thickness Constraint

Simon Painchaud-Ouellet[*], **Christophe Tribes**[†], **Jean-Yves Trépanier**[‡], **and Dominique Pelletier**[§]
École Polytechnique de Montréal,
2900, boulevard Édouard-Montpetit, Campus de l'Université de Montréal,
Montréal (Québec), H3T 1J4, Canada.

Results for 2D airfoil shape optimization in transonic regime are presented. A Navier-Stokes flow solver is used to compute the flow-field. Single-point and multipoint formulations of the optimization problem are proposed and compared. A NURBS representation of the airfoils allows smooth optimized airfoils to be obtained which do not experience severe performances losses in off-design condition. The multipoint formulation, combined with the NURBS representation, allows to obtain airfoils with good performance over a specific Mach range. A design of experiment is conducted to determine the most sensitive design variables in order to reduce their number in the optimization process.

1. Introduction

Airfoil shape optimization using computational fluid dynamics (CFD) has attracted much effort in the past years. Better access to powerful computer resources, the development of reliable optimization techniques and of accurate and faster CFD codes have allowed aerodynamicists to push forward the development of new airfoils.

There are many ways to formulate the optimization problem; one possible way is the *Target* Cp formulation, where the design engineer fixes a target Cp curve and tries to obtain an airfoil that has a Cp curve matching the target curve. This formulation requires a perfect knowledge of transonic aerodynamics in order to define target curves that are physically relevant, and whose corresponding airfoils will indeed provide good aerodynamic properties. Therefore, even if this formulation has been widely used in industry, its dependency on the engineer's experience makes it very delicate to use.

A second formulation of the problem, the *Drag Reduction* formulation, works directly on reducing the drag of an airfoil. The objective is to obtain the airfoil that minimizes drag (Cd) for a given lift (Cl^*) at a given flight condition *i.e.* Mach number (M_∞). However, many problems have been encountered while using this formulation: unrealistic airfoils, "bumpy" airfoils, and shapes with poor off-design performance were obtained.[2,3,11] It appears that the *Drag Reduction* formulation can be even more difficult to use than the *Target* Cp formulation. However, because of its great design possibilities, much work has been conducted to overcome the problems associated with the *Drag Reduction* method.

One of the main problems observed when conducting drag minimization is that airfoils produced by the optimizers for transonic flow regimes have good performance at a very specific flight condition, but behave poorly as soon as this flight condition changes. This behavior, also referred to as localized optimization, is due to the optimizers' ability to create bumps on the upper surface of the airfoil. These bumps are helping to strongly reduce the shock for a specific Mach number, but are detrimental at any other flight condition.

One objective of the present work is to use a more global geometric representation of the airfoils in order to prevent localized optimization problems observed in previous studies. The NURBS representation, by using fewer control points to define an airfoil, is able to prevent formation of local bumps because each of the control points has a more global influence on the definition of the airfoil. Furthermore, we will illustrate the differences between optimizing for a given Mach number (single-point formulation) and for a set of Mach numbers (multipoint formulation).

The effects of the shock on the boundary-layer can only be fully accounted with a Navier-Stokes flow solver, allowing a more accurate drag computation. Since the objective of airfoil shape optimization is to minimize the drag of an airfoil, it is important to get as much accuracy on the drag as is possible. Therefore, a Navier-Stokes flow solver is used to compute viscous and compressible effects on airfoils.

Optimizations are conducted with a transonic airfoil as initial design and a thickness constraint is imposed.

[*]Graduate Student, École Polytechnique de Montréal, simon.painchaud-ouellet@polymtl.ca
[†]Research Associate, École Polytechnique de Montréal, christophe.tribes@polymtl.ca
[‡]Professor, Department of Mechanical Engineering, École Polytechnique de Montréal, jean-yves.trepanier@polymtl.ca
[§]Professor, Canada Research Chair, Department of Mechanical Engineering, École Polytechnique de Montréal, dominique.pelletier@polymtl.ca

Copyright © 2004 by the authors. Published by the American Institute of Aeronautics and Astronautics, Inc., with permission.

2. Aerodynamics in Transonic Regime

Airfoils in the transonic regime are continuously studied by engineers mainly because most commercial aircrafts operate in this regime. An airfoil enters the transonic regime when local supersonic regions appear on the suction side. The Mach number for which this happens (also referred to as the critical Mach number, or M_{cr}) varies from airfoil to airfoil, and its value is around $M_{cr} \approx 0.7$.

At higher Mach numbers, a shock usually appears on the upper surface which increases significantly the drag on the airfoil for two reasons. First, the loss of total pressure across the shock causes *wave drag*. Second, when M_∞ reaches $M_{drag-divergence}$, the shock is strong enough to cause separation of the boundary layer at the foot location of the shock. The flow separation causes total drag on the airfoil to increase significantly. This is known as the *drag divergence*.[1] Aircrafts operating in the transonic regime are usually designed so that the operating point is before the occurrence of the drag divergence.

3. Localized Optimization

Recent work has been reported by Huyse *et al.*[3] on the drag reduction problem for a NACA0012 airfoil in the transonic regime. The airfoil was parameterized by splines using 23 control nodes and a Euler CFD code was used to get flow solutions. The main objective was to obtain optimized airfoils that perform well on a certain Mach range, and their efforts were placed on the formulation of the optimization problem.

The most obvious formulation of the problem is the *single-point* formulation, where drag (Cd) is reduced at constant lift (Cl^*) for a specific flight condition (M_∞). Huyse *et al.* observed that the optimizer is capable of taking advantage of the flow-field condition to reduce the drag on the airfoil: a "bump" is introduced at the exact foot location of the shock on the suction side in order to suppress this shock. However, the foot location of the shock moves with M_∞, and the bump becomes totally ineffective as M_∞ changes. Therefore, single-point optimization leads to airfoils with poor off-design performance. This type of localized optimization associated with bumps had also been reported by Drela.[2] Figure 1 shows Huyse's results for the single-point optimization.

Aircrafts are expected to have good performance over a given Mach range. Therefore, Huyse *et al.* concluded that the single-point approach could not allow such airfoils to be generated, and tried a multipoint approach. In this approach, every airfoil generated by the optimizer is evaluated for a set of k flight conditions, and the sum of the drags at the k different Mach numbers ($M_{\infty,i}$) is minimized. Figure 2 shows Huyse's results for 2 multipoint optimizations.

Huyse *et al.* observed that the multipoint approach

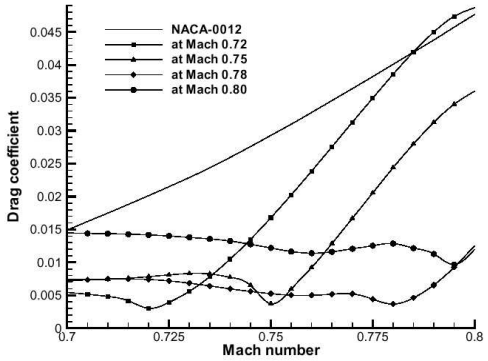

Fig. 1: Cd *vs* Mach for single-point optimizations using various design Mach numbers, Cl* = 0.6 (from Huyse *et al.*[3])

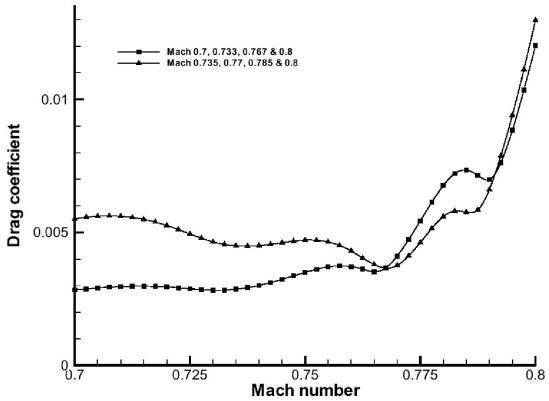

Fig. 2: Cd *vs* Mach for multipoint optimizations using various design Mach numbers, Cl* = 0.6 (from Huyse *et al.*[3])

leads to airfoils with k small bumps on the extrados, placed at the foot location of the shocks associated with the k Mach numbers. Therefore, the multipoint formulation computed airfoils with better performances for the given set of Mach numbers, but still had unsatisfactory performances over the entire Mach range.

To remedy the wavy behavior of the Cd *vs* Mach curves (Figures 1 and 2), Huyse *et al.* have proposed a formulation of the optimization problem that combines the multipoint formulation with a statistical approach, and their results were conclusive.[3]

The current work will explore a different approach to the drag reduction problem by focusing on the effects of the geometric representation. We will try to demonstrate that a NURBS representation can be used in the optimization process to obtain smoother airfoils that will not experience severe performance degradation at off-design conditions.

4. NURBS Representation of Airfoils

A NURBS (Non Uniform Rational B-Spline) is built on fraction of the B-spline interpolation functions. NURBS curves are defined, in a parametric form, by:

$$\mathbf{C}(u) = \sum_{i=0}^{n} R_{i,p}(u)\mathbf{P_i}$$

with

$$R_{i,p}(u) = \frac{N_{i,p}(u)\omega_i}{\sum_{j=0}^{n} N_{j,p}(u)\omega_j}$$

where the $\mathbf{P_i}(x_i, y_i)$ are the control points (Figure 3), ω_i their associated weights, $N_{i,p}$ the p-th degree B-spline basis function and $\mathbf{C}(u)$ a vector-valued function giving the position on the curve relative to a parameter u.

Using a NURBS parameterization ensures curvature continuity of the airfoil geometric representation. The higher the order of the basis functions and the higher the order of the curvature continuity. Basis functions of degree 3 — order 4 — have been considered here for airfoil shape parameterization; this corresponds to polynomial curves with cubic terms in the NURBS representation.[a]

The regularity property of the geometric representation depends also on the number of control points. Associated with the control points are zones of influence which overlap locally along the curve. Even though, the order of the NURBS modifies the extent of the zone of influence, it has been kept constant to maintain curvature continuity, but the number of control point has been selected according to the complexity of the airfoil shape considered. Thus, the number of control point must be selected to satisfy a compromise between smoothness and representation accuracy.

The efficiency of NURBS for representing airfoil profiles and its applicability to shape optimization have been discussed by Lépine *et al.*[4] A large variety of airfoils (RAE2822, Boeing A4, Boeing A8, Bombardier-Canadair) can always be represented with 13 control points or fewer, with an accuracy of $\epsilon_{max} \leq$ 8E-5. This accuracy has been found sufficient to comply with manufacturing tolerance and flow solver sensitivity. For example, 10 control points would be enough to reach this accuracy for the NACA0012 airfoil, which is easy to represent since it is symmetric and not cambered. The transonic airfoil we have considered here as initial design is a more complex shape and necessitates 13 control points in order to obtain the desired accuracy (see Fig. 3).

Since NURBS representation of airfoils relies on few design parameters, the risk of noise in the representation of the airfoil is significantly reduced. Thus, this method makes the aerodynamic optimization process easier because the NURBS representation of the airfoil is naturally constrained to have good regularity properties. Finally, in a drag minimization perspective, the low number of control points required to represent an airfoil with a NURBS prevents the creation of "bumpy" airfoils and accelerates the optimization process.

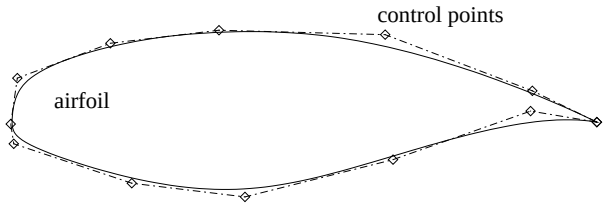

Fig. 3: Representation of a transonic airfoil using 13 control points

The methods adopted to manipulate NURBS representation use some of the classes of the *Pirate*[b] library for software development.

5. Flow Solver and Grid Convergence

A Navier-Stokes flow solver is used for the evaluations of Cl and Cd. The importance of viscous effects in the transonic regime justifies its use. The CFD code selected is NSU2D,[5] an unstructured mesh compressible Reynolds-averaged Navier-Stokes solver designed principally for steady-state solutions in the transonic and subsonic regimes for single and multielements airfoils.

Grid resolution will influence both the precision of the solution obtained from the solver and the computation time. In an optimization process where many calls to the solver will be required, it is important to find a grid resolution that will provide satisfactory resolution for the lowest possible computation time. Moreover, NSU2D uses iterative steps, or cycles, to reduce the error of the solution. Therefore, the number of cycles used is also a parameter affecting the quality of the solution and the computing time. In order to select an acceptable compromise, a convergence study that considers the effects of the grid resolution and the number of cycles has been conducted.

It has been concluded that using a grid with 25000 elements and 150 cycles is the combination where the solution requires the less computation time while providing a satisfactory solution. This combination will therefore be used in the optimization process.

[a] For more details about the NURBS, their properties and the way they are obtained please refer to *The NURBS Book*.[8]

[b] see `http://www.polymtl.ca/grmiao/grmiao/` for online documentation

6. Airfoil Shape Optimization

A general mathematical statement for an optimization problem is given as follows:

$$\begin{aligned} &\min_{\mathbf{d}} F(\mathbf{d}) \\ \text{subject to: } &\mathbf{g}(\mathbf{d}) \geq 0 \\ &\mathbf{h}(\mathbf{d}) = 0 \end{aligned}$$

This problem, in the case where F, g and h are differentiable functions, is efficiently solved by a SQP (*Sequential Quadratic Programming*) algorithm[9,12] implemented in **DONLP** under the iSIGHT 7.0 environment, a product of Engineous Software.

The selection of the optimizer is, in the present case, almost arbitrary since it is considered to be a black box that returns an optimized design for a given formulation of the problem (design variables selection, objective function and constraints expression) and for given initial values of the design variables. Although this choice is not definitive because other approaches exist or will probably be developed, it has been preferred to consider a gradient-based optimizer able to handle inequality constraints and whose implementation in an optimization process could be readily modified.

Gradient-based methods have been used widely, but one must keep in mind that the optimum obtained is a global optimum if the objective and constraints are differentiable and convex. However, typical aerodynamic objectives are not necessarily smooth.[10] With well defined gradient, only a local optimum in the neighborhood of the initial point can be obtained. Therefore, we expect to obtain optimized airfoils whose shape will be similar to that of the initial airfoils. Only global optimization algorithms would allow to find a new family of airfoils, but these kinds of optimizers are much too time consuming to use. Moreover, the use of a gradient-based method can be justified in a more practical way: when aerodynamic optimizations are conducted on airfoils in the industry, the objective is to improve an existing airfoil that is already efficient. In that case, the optimum would be near the initial airfoil, and a gradient-based method would allow to find it efficiently.

Several aspects are critical when formulating an optimization problem: selecting and scaling the variables, providing sensitivity analysis and defining the objective function and the constraints. These aspects will be reviewed in the next subsections.

6.1. Selecting and scaling variables

The initial transonic airfoil we have considered is represented with 13 control points, 2 being fixed at the trailing edge of the airfoil. Each of the free control point $\mathbf{P_i}$ has 3 associated components: x, y and ω, leading to possibly 33 design variables in the optimization process. The SQP method requires gradient evaluation of the functions at each iteration of the optimization process. Since finite difference expressions are used for gradient evaluations, results could take too much time to be obtained with 33 design variables

In order to reduce the number of design variables, a design of experiment is performed at $M_\infty = 0.73$, which corresponds to the middle of the Mach range studied for this airfoil. The x components of the control points near the leading edge are kept fixed as constants for solver stability. The 13 most sensitive variables, as found with the design of experiment, are selected to be the design variables and are shown on Figure 4.

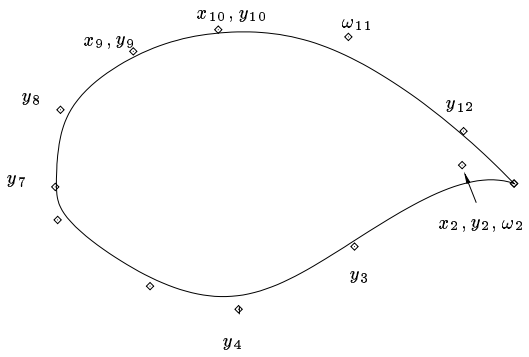

Fig. 4: Design variables selected with the design of experiment

For SQP methods, it is desirable to have the same order of magnitude for the design variables since gradients of the cost function $\nabla F(\mathbf{X})$ are computed to find a descent direction. Good scaling can be achieved with the usage of dimensionless variables.

The optimizer will modify the scaled variables without consideration for the nature of the variable. Therefore, it is important that the scaling reflect the same importance of variation for all variables. After experimentation, scaling has been chosen so that a variation of the scaled variable between ± 1 yields an equivalent ± 5 % variation of the chord for the x variables and of the maximum thickness for the y. The scaling for the x_i and y_i components are therefore:

$$\begin{aligned} Y_i &= 150(y_i - y_o) \\ X_i &= 20(x_i - x_o) \end{aligned}$$

The scaling of the weights ω_i components is different since the weights affect the airfoil definition in a logarithmic way instead of linearly. The scaling chosen is the following:

$$\Omega_i = \frac{1}{\ln(2)} \ln\left(\frac{\omega_i}{\omega_o}\right)$$

This scaling ensures that for Ω_i = -1 and $\Omega_i = 1$, the actual corresponding values of ω_i will be respectively $\omega_i =$

$0.5\omega_o$ and $\omega_i = 2\omega_o$, which correspond to a ± 5 % variation of the maximum thickness of the initial airfoil.

After scaling, the design vector for this study is $\mathbf{d} = \{X_2,X_9,X_{10},Y_2,Y_3,Y_4,Y_7,Y_8,Y_9,Y_{10},Y_{12},\Omega_2,\Omega_{11}\}$.

6.2. Determination of the differentiation step size

SQP optimizers first determine a desired search direction that minimizes a quadratic approximation of the objective function subject to linear approximations of the constraints. Both approximations require derivative with respect to each design variable. The evaluation of the gradients of F, g and h is critical to find a good search direction. The numerical differentiation is done using forward finite difference:

$$\frac{\partial F}{\partial d_i} = \frac{F(d_i + h) - F(d_i)}{h}$$

where h is the differentiation step size and is fixed by the user. The choice of the differentiation step size has to be done very carefully to ensure the accuracy of the gradients, especially when functions with numerical noise are to be differentiated. Coarser differentiation step sizes provide gradients that are less affected by numerical noise, but also cause losses in gradients accuracy. We chose a successive step size strategy in our optimization process: a coarse step size is used at first to help the optimizer explore larger zones of the design space and to help overcome local minima of the function F. The airfoil found is then used as a new initial airfoil and a finer step size is used (half of the previous one) in a new optimization process. The finer step size allows the optimizer to explore more locally around the new airfoil. The process is repeated until the step size reaches the order of the numerical noise, which had been determined *a priori* in a sensitivity analysis.

6.3. Separating α from the geometric variables

The original single-point formulation of the drag minimization problem is the following:

$$\begin{aligned} \min_{\alpha,\mathbf{d}} \quad & Cd(\mathbf{d},\alpha,M_\infty) \\ \text{s.t.:} \quad & Cl(\mathbf{d},\alpha,M_\infty) \geq Cl^* \\ & \text{+ geometric constraints} \end{aligned}$$

where α is the angle of incidence of the flow relative to the $\mathbf{x}$ axis. Obviously α does not influence the representation of the airfoil, but with the parameterization presented in the § 4, the true angle of attack of the airfoil relative to the flow-field depends on $\mathbf{d}$. In order to make clear the role of each design variable, we have decided to rescale and rotate the airfoil such that, independently of $\mathbf{d}$, the trailing edge is always located at (1,0) and the geometric leading edge[c] is located at (0,0). Thus, when using this procedure, $\mathbf{d}$ does not impact on the angle of attack of the rescaled airfoil relative to the flow-field. In addition, the geometric constraints depends now only on $\mathbf{d}$.

A few tests with the original formulation have shown that the optimizer has some difficulties to improve the design.[7] We explain this behavior by the fact that the coupled influence of α and $\mathbf{d}$ on Cd and Cl must be extremely non-linear, and the optimizer can make only very small steps in the design space because the descent direction is valid only in the vicinity of the considered design point.

However, a simple aerodynamic relation between α, lift and drag can justify the separation of α from the geometric variables in the formulation of the optimization problem. By fixing $\mathbf{d}$ as a parameter, the original formulation becomes a sub-problem which is written as follows:

$$\begin{aligned} \min_{\alpha} \quad & Cd(\mathbf{d},\alpha,M_\infty) \\ \text{s.t.:} \quad & Cl(\mathbf{d},\alpha,M_\infty) \geq Cl^* \end{aligned}$$

α is not concerned by the geometric constraints and they are removed from the sub-problem. Moreover, for a vast majority of non-stalled airfoils, increasing α leads to larger in Cl and Cd. Therefore, finding α so that Cl is as close as possible to Cl^* will ensure that Cd is minimized for a specific airfoil while respecting the lift constraint in the problem formulation. Thus, the sub-problem considered is written as follows:

$$\begin{aligned} \min_{\alpha} \quad & \alpha \\ \text{s.t.:} \quad & Cl(\mathbf{d},\alpha,M_\infty) \geq Cl^* \end{aligned} \tag{1}$$

In the master problem, $\mathbf{d}$ are the design variables. Although the angle of incidence of the flow influences the drag it is not used as a design variables to reduce the drag. In this formulation, α is found by the sub-optimization so that every airfoil generated by the optimizer in the master optimization satisfies the lift constraint. The master problem is now written as:

$$\begin{aligned} \min_{\mathbf{d}} \quad & Cd(\mathbf{d},\alpha,M_\infty) \\ \text{s.t.:} \quad & \text{geometric constraints} \end{aligned} \tag{2}$$

The master optimizer now only works on reducing the drag, the lift constraint being always satisfied via the sub-optimization. However, the sub-optimization requires many solver calls (around 5 or 6) for each evaluation of Cd required by the master problem, thus increasing the computing time to evaluate the objective function and the constraint function compared with the non-separated formulation.

[c] It has been considered that the "geometric" leading edge is the point of the airfoil the most distant to the trailing edge.

6.4. Expressing the geometric constraint

A preliminary study was conducted with a NACA0012 as initial airfoil.[6,7] The optimization problem is formulated as the one given in Eq. 1 and 2. The difference is that $\mathbf{d} = \{Y_2, \ldots, Y_{10}\}$ and the geometric constraints are bound constraints on the design variables: the y coordinates of the control points cannot move by more than 20 % of their initial value. The intent was to prevent the optimizer from obtaining very thin airfoils and to avoid geometries such that the upper surface crosses the lower surface. The optimizer grasps the importance of getting slimmer airfoils to reduce the drag. The optimized airfoils are thinner than the initial airfoil (10.5 % instead of 12 % of the chord length), and they would have been even thinner if the design variables had not been bounded. This trend has raised the necessity to introduce thickness constraints on the airfoil to take into account, in a first approximation, the volume constraint imposed by structural components on a wing skin.

For the current work, the maximum thickness of the airfoil is controlled explicitly through a constraint in the formulation of the optimization problem: $(t/c)_{max} \geq (t/c)^*_{max}$ where $(t/c)^*_{max}$ is the maximum thickness of the initial airfoil.

7. Optimization Formulation and Results

7.1. Single-point optimization

The single-point optimization problem is the following:

$$\begin{aligned} \min_{\mathbf{d}} \quad & Cd(\mathbf{d}, \alpha, M_\infty) \\ \text{s.t.:} \quad & (t/c)_{max} \geq (t/c)^*_{max} \end{aligned} \tag{3}$$

still subject to the subproblem:

$$\begin{aligned} \min_{\alpha} \quad & \alpha \\ \text{s.t.:} \quad & Cl(\mathbf{d}, \alpha, M_\infty) \geq Cl^* \end{aligned}$$

Three single-point optimizations are conducted separately for 3 flight conditions: $M_\infty = 0.705$, $M_\infty = 0.73$ and $M_\infty = 0.755$ with $Re = 1E6$. These flight conditions were chosen because $M_\infty = 0.73$ is the design point for the initial airfoil, and we wanted to study a Mach range of [0.68-0.78]. The chosen constraints are $Cl^* = 0.8$ and $(t/c)^*_{max} = 0.12$, which correspond to the lift of the initial airfoil at $M_\infty = 0.73$ and $\alpha \approx 2.5^o$ and to the maximum thickness of the initial airfoil.

Figure 5 illustrates that optimized airfoils are very smooth. The optimized airfoils reduced the strength of the shock without creating bumps on the upper surface of the airfoil. The optimizer was able to handle the thickness constraint since all optimized airfoils have a maximum thickness above 0.12. It can be noted that the higher the Mach number, the more important is the difference with the initial airfoil. For high Mach number the optimization tend to flatten the upper surface while accentuating the curvature change of the lower surface. This is a characteristic of supercritical airfoils.

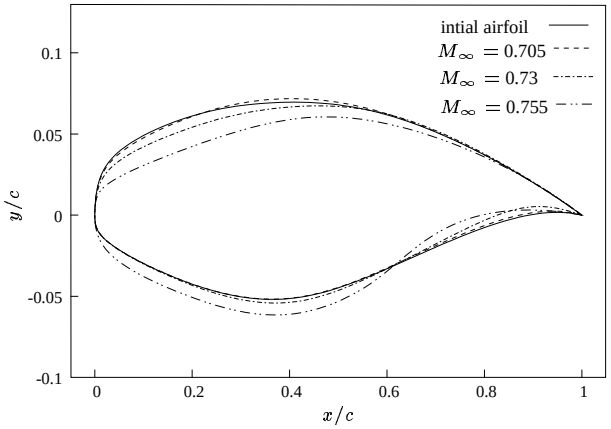

Fig. 5: Initial transonic airfoil and single-point optimized airfoils at $\mathbf{M_\infty = 0.755}$, $\mathbf{M_\infty = 0.705}$ and $\mathbf{M_\infty = 0.73}$

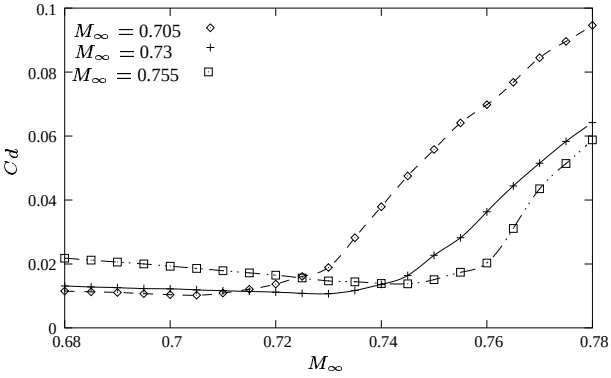

Fig. 6: $\mathbf{Cd}$ *vs* $\mathbf{M_\infty}$ for initial and single-point optimized airfoils, $\mathbf{Cl^* = 0.8}$

The optimizer was able to capture the influence of the shock and its action on the boundary layer so as to minimize the drag at constant lift. Figures 7(a) and 7(b) illustrate how the shock is diminished after optimization at $M_\infty = 0.705$ and $M_\infty = 0.73$. For these two flight conditions, the gains in Cd are 23.9% and 49.8% respectively (see the single-point optimization results in Table 1), which is quite important considering that the initial airfoil is already well adapted for transonic regime. Figures 8(a) and 8(b), show that the boundary layer is kept attached by the optimization. It can be observed that friction drag is slightly increased by the optimization, thus the gain in total drag is mainly due to the reduction

of wave drag.

The Cp curve at $M_\infty = 0.755$ (see Fig. 7(c)) shows that the shock is moved downward by the optimization, but the amplitude of the shock is similar before and after optimization. However, the gain in Cd for this flight condition is 76.7% and is mainly due to the reduction of the form drag. As can be seen on Figure 8(c), before optimization the boundary layer on the upper surface was separated, resulting in negative friction coefficient downstream $x/c = 0.4$ and high form drag. After optimization, the boundary layer is attached on the upper surface — and the lower surface —, resulting in lower form drag. For this case, the optimizer seizes the influence of boundary layer effects on the total drag coefficient. Thus, using a Navier-Stokes flow solver permits to find design well suited for flight condition where form drag is dominating on total drag due to the interaction between shock wave and boundary layer. One can also observe on Figure 8(c) that friction drag is increased during optimization.

The optimized airfoils provide Cd *vs* M_∞ curves with smooth off-design transition as shown on Figure 6. A "mild" local minimum is found at the design point for the three optimized airfoils . However, the localized effects are still much less pronounced than what has been observed in past work on the subject (see Fig. 1).

7.2. Multipoint optimization

Although the three airfoils obtained in the previous section were all smooth, there shape was depending on Mach number and their drag-rise behavior was different. In order to find the best airfoil for a given Mach range, one must consider multipoint optimizations.

In practice, only information for specific discrete regimes can be obtained, thus, one must select few flight conditions covering the entire range. After that, the trade-off between the different flight conditions can be expressed as a multi-objective optimization problem — or vector-optimization problem. Typically, there is no single global solution for such a problem. For example, according to the importance given to each flight condition, the optimal design can be different.
But, in our case, the importance of each flight condition is known *a priori*, also each objective has the same nature and all objectives are commensurable. In such case, it is advantageous to transform the original vector objective function by a scalarization methods that defines which compromise should be made. The idea is to create a scalar objective function out of the vector objective function. First, each objective is normalized with its initial value. Second, a scalar objective function must be defined. A simple way to do that is to sum all the objectives. The preference given to each objective is expressed as a weighting factor in the summation. The compromise objective function is written as:

$$F_{comp} = \sum_{i=1}^{k} w_i \left[\frac{Cd_i(\mathbf{d}, \alpha_i, M_{\infty,i})}{Cd_i^o} \right]$$

These two transformations lead to the proposed multipoint formulation of the airfoil shape optimization problem:

$$\begin{aligned} \min_{\mathbf{d}} \quad & \sum_{i=1}^{k} w_i \left[\frac{Cd_i(\mathbf{d}, \alpha_i, M_{\infty,i})}{Cd_i^o} \right] \\ \text{s.t.:} \quad & (t/c)_{max} \geq (t/c)^*_{max} \end{aligned}$$

subject to the k subproblems:

$$\begin{aligned} \min_{\alpha_i} \quad & \alpha_i \\ \text{s.t.:} \quad & Cl(\mathbf{d}, \alpha_i, M_{\infty,i}) \geq Cl^* \end{aligned}$$

An experiment with the same constraints as in the single-point formulation is conducted ($Cl^* = 0.8$ and $(t/c)^*_{max} = 0.12$). Three flight conditions ($Re = 1E6$) are considered: $M_{\infty,1} = 0.705$, $M_{\infty,2} = 0.73$ and $M_{\infty,3} = 0.755$, each of them weighted equally ($w_i = 1$). This means that the airfoil would operate at each M_∞ in an equal proportion of time. We chose this condition because it corresponds to a worst case scenario, making the optimization process even harder. In a more practical case, if the design point of the airfoil were, for example, $M_\infty = 0.73$, we could choose the same $M_{\infty,i}$ with weights based on a normal distribution of the flight conditions as discussed by Huyse.[3] The number of flight conditions can also be changed, but a higher value of k will lead to a longer optimization process since every airfoil generated has to be evaluated at those k Mach numbers.

Figure 9 depicts the multipoint optimized airfoil. One can easily observe that it is as smooth as the initial airfoil and that the upper surface is flatten and the curvature change of the lower surface is accentuated.

Table 1 shows the results obtained by the single-point and the multipoint formulation. As expected, in terms of the compromise objective function, the multipoint-optimized airfoil performs better than each of the single-point optimized airfoil: the gain is 49.5% with the multipoint formulation (emphasized number in the right column of the table) compared with 16.4%, 41.1%, 22.5% for the single-point formulation at $M_\infty = 0.705$, $M_\infty = 0.73$, $M_\infty = 0.755$ respectively. Thus, the multipoint approach produces an airfoil with better performance over the Mach range than any airfoil obtained with the single-point formulation. Contrary to the single-point optimization, localized effects are no longer visible on the Cd *vs* M_∞ curve, as shown on Figure 10.

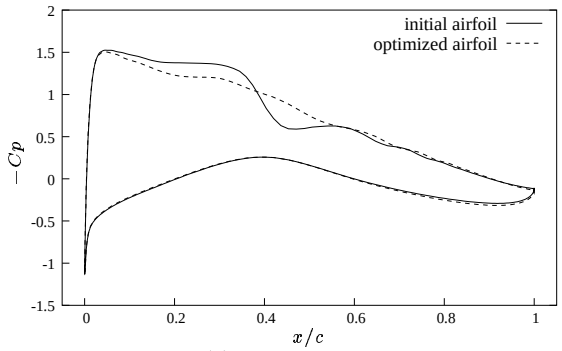

(a) $\mathbf{M}_\infty = 0.705$

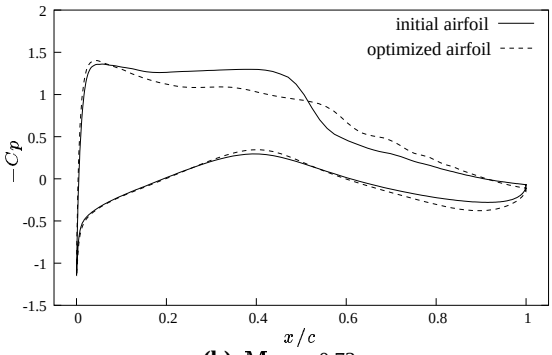

(b) $\mathbf{M}_\infty = 0.73$

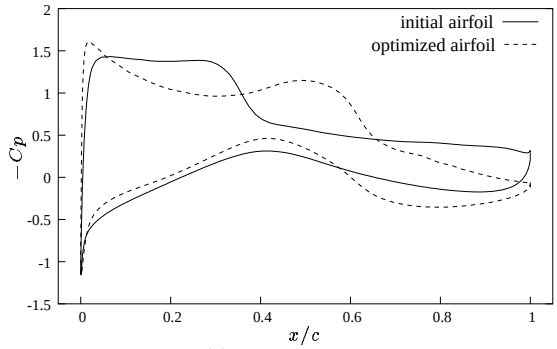

(c) $\mathbf{M}_\infty = 0.755$

Fig. 7: Cp curves for the initial airfoil and the single-point optimized airfoil at various Mach number

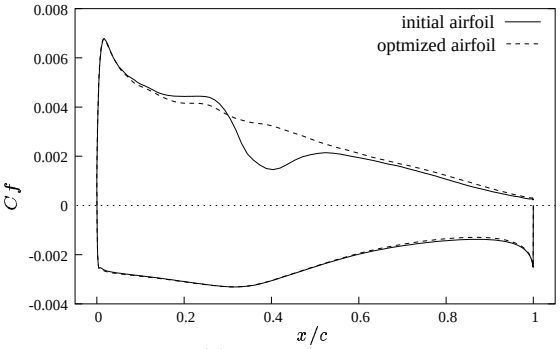

(a) $\mathbf{M}_\infty = 0.705$

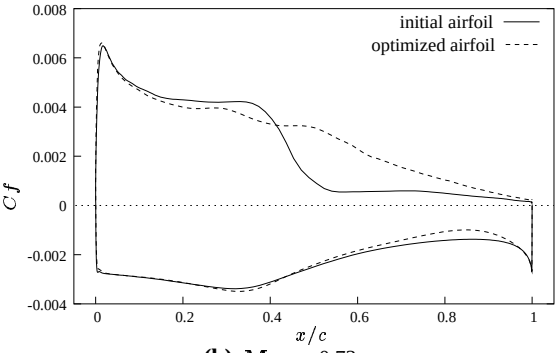

(b) $\mathbf{M}_\infty = 0.73$

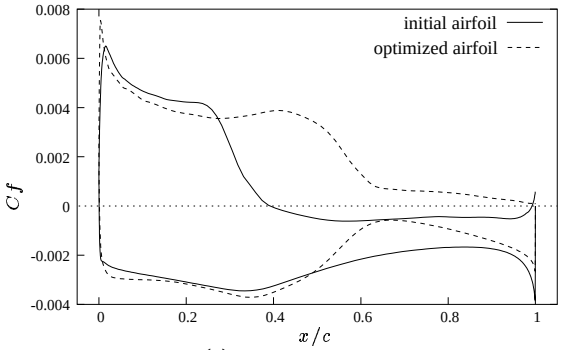

(c) $\mathbf{M}_\infty = 0.755$

Fig. 8: Cf curves for the initial airfoil and the single-point optimized airfoil at various Mach number

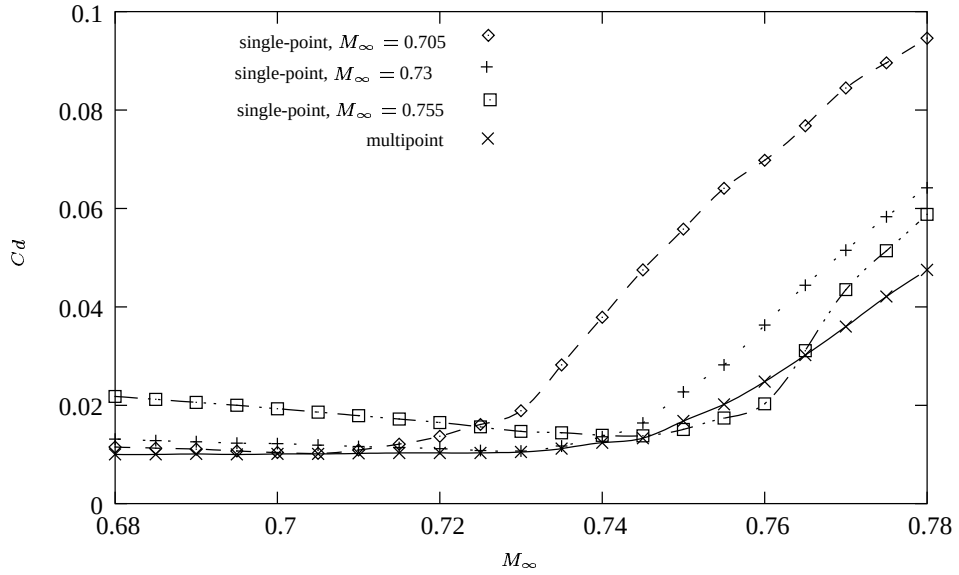

Fig. 10: Cd *vs* M_∞ for the multipoint and single-point optimized airfoils, $Cl^* = 0.8$

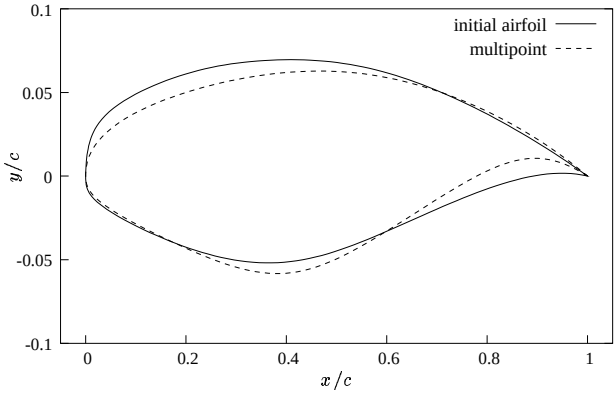

Fig. 9: Initial airfoil and multi-point optimized airfoil

However, when comparing Cd obtained with the different formulations it is surprising to observe that the multipoint-optimized airfoil performs better at $M_\infty = 0.705$ and $M_\infty = 0.73$ than the single-point optimized airfoils at the corresponding Mach number. The difference is very small at $M_\infty = 0.705$: $Cd = 0.0101$ with the multipoint *vs* $Cd = 0.0102$ with the single-point at $M_\infty = 0.705$. Almost the same difference is observed at $M_\infty = 0.73$. On the contrary, for $M_\infty = 0.755$, the single-point optimized airfoil at $M_\infty = 0.755$ performs better than the multipoint optimized airfoil. This behavior can be explained by the fact that the single-point optimization can stop prematurely at a solution that the multipoint optimization can surpass eventually.

Cp curves on Figure 11(a) show a weak shock that is present with the multipoint optimized airfoil at $M_\infty = 0.705$ while it is absent with the single-point optimized airfoil. On Figures 11(b) and 11(c) it is interesting to note that Cp curves are typical of supercritical airfoils with large constant pressure plateaux on the upper surface. As for the friction coefficient, the curves are similar to those obtained with single-point optimization (see Fig. 12(a) to 12(c)).

Optimization history for the different formulations is illustrated on Fig. 13. With single-point optimization, the higher the Mach number, the more iterations are required; this trend is related to the difficulty to diminish drag associated with the shock wave as the Mach number is increased. Obviously, the multipoint optimization combines all the difficulties of the single-point optimization in addition of finding a good compromise between all the regimes. This results in a slower convergence.

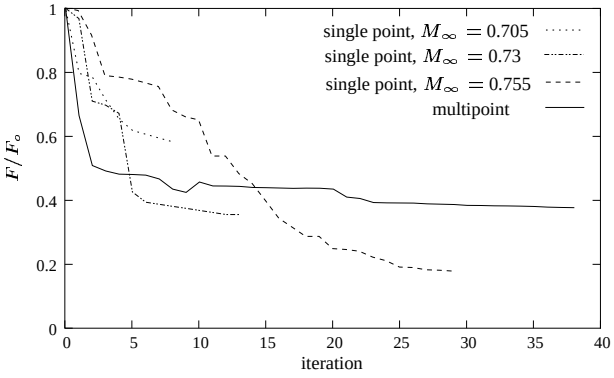

Fig. 13: Optimizations history

8. Conclusion

In this work, we have discussed how NURBS representation can help to obtain smooth airfoils in a drag minimization process.

	($M_\infty = 0.705$)		($M_\infty = 0.73$)		($M_\infty = 0.755$)		($M_\infty = 0.705, 0.73, 0.755$)	
	Cd	(gain)	Cd	(gain)	Cd	(gain)	$F_{comp}/3$	(gain)
initial airfoil	0.0134	-	0.0213	-	0.0746	-	1	-
single-point ($M_{\infty,1} = 0.705$)	0.0102	23.9%	0.0189	(11.3%)	0.0641	(14.1%)	0.836	(16.4%)
single-point ($M_{\infty,2} = 0.73$)	0.0119	(11.2%)	0.0107	(49.8%)	0.0282	(62.2%)	0.589	(41.1%)
single-point ($M_{\infty,3} = 0.755$)	0.0186	(-38.8%)	0.0147	(31.0%)	**0.0174**	**(76.7%)**	0.775	(22.5%)
multipoint	**0.0101**	**(24.6%)**	**0.0105**	**(50.7%)**	0.0202	(72.9%)	**0.505**	**(49.5%)**

Table 1: Cd at different $\mathbf{M}_\infty$ for the initial and the optimized airfoils

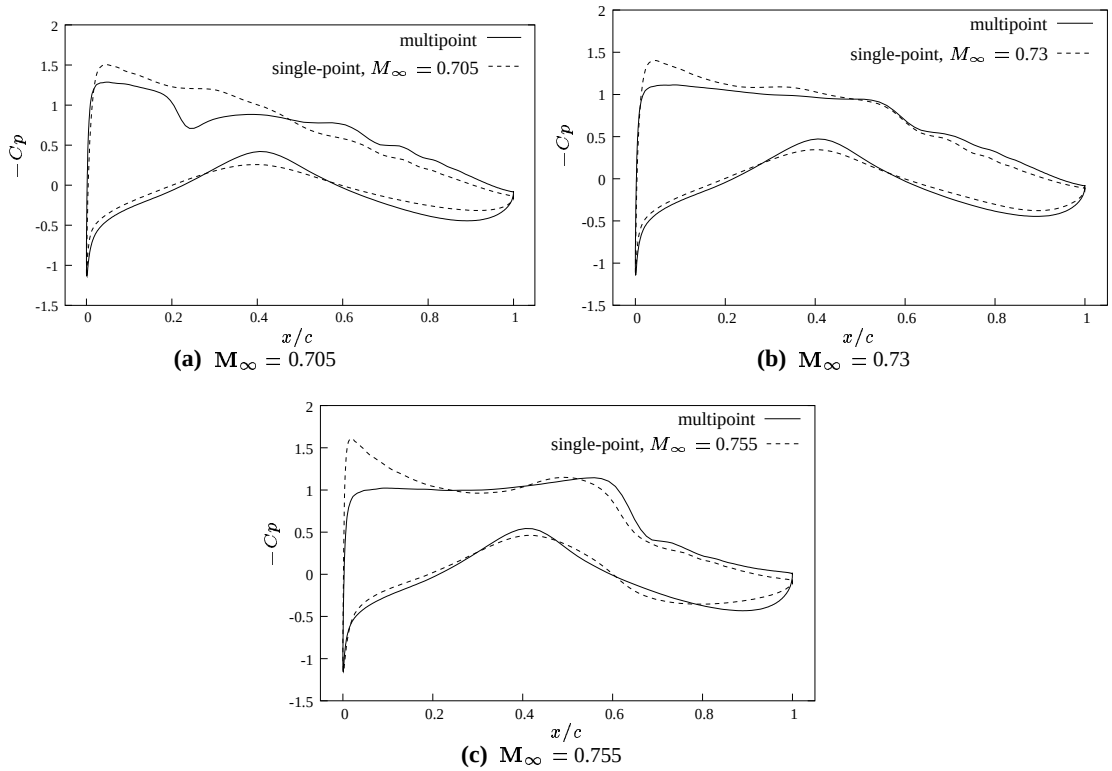

(a) $\mathbf{M}_\infty = 0.705$ **(b)** $\mathbf{M}_\infty = 0.73$ **(c)** $\mathbf{M}_\infty = 0.755$

Fig. 11: Cp curves for the initial airfoil and the multipoint optimized airfoil at various Mach number

A design of experiment was conducted to select the most sensitive design variables and reduce their number.

In order to avoid extremely thin airfoil, an explicit constraint on the maximum relative thickness was implemented.

A bi-level formulation of the optimization problem is proposed. A separation of the design variables in two groups is done, and each group is assigned a specific task. For the subproblem, the angle of attack serves for satisfying a constraint on the expected lift. The control points of the NURBS are more specifically intented for total drag reduction in the master problem.

Even when used with a single-point formulation, the NURBS are able to provide airfoils with gentle changes in off-design flight conditions. Using a Navier-Stokes flow solver enables to take into account not only the wave drag, but also the drag associated with the interaction between the shock wave and the boundary layer. This seems to have an impact on the optimized airfoil when the flight condition approaches the drag divergence region.

It has been observed that the single-point optimized airfoil shows some Mach number dependency, and that the corresponding Cd *vs* M_∞ curves presents a mild minimum for this value. The multipoint formulation, even though it is more costly, prevents this behavior.

For the case considered here, the multipoint optimized airfoil is smooth with good performance over the specified range of flight conditions.

Acknowledgments

This work was supported in part by NSERC (Government of Canada), FQRNT (Government of Québec) and the Canada Research Chair Program (Government of Canada).

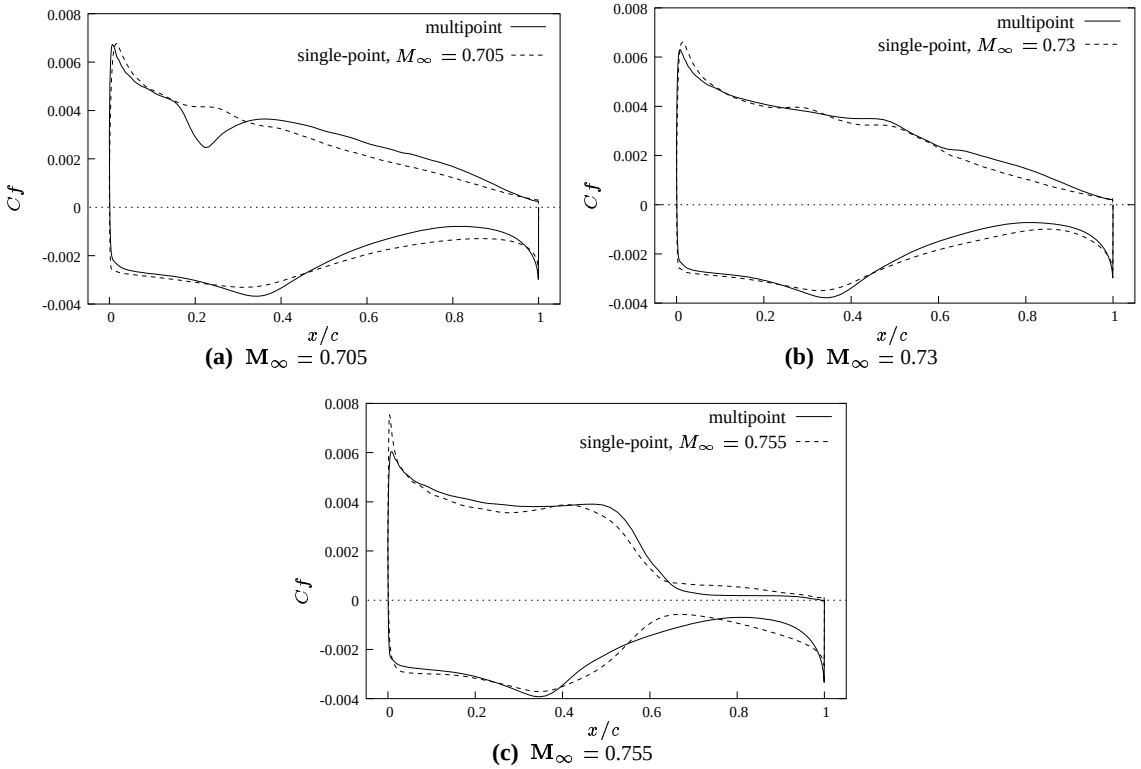

(a) $\mathbf{M}_\infty = 0.705$ **(b)** $\mathbf{M}_\infty = 0.73$ **(c)** $\mathbf{M}_\infty = 0.755$

Fig. 12: Cf curves for the initial airfoil and the multipoint optimized airfoil at various Mach number

References

[1] J. D. Anderson, Jr. *Modern Compressible Flow*. McGraw-Hill Publishing Company, 2nd edition, 1990.

[2] M. Drela. Pros and cons of airfoil optimization. In D. Caughey and M. Hafez, editors, *Frontiers of Computational Fluid Dynamics*, pages 363–381. World Scientific, 1998.

[3] L. Huyse, S. L. Padula, R. M. Lewis, and W. Li. Probabilistic approach to free-form airfoil shape optimization under uncertainty. *AIAA J.*, 40(9):1764–1772, September 2002.

[4] J. Lépine, F. Guibault, J.-Y. Trépanier, and F. Pépin. Optimized NonUniform Rational B-Spline geometrical representation for aerodynamic design of wings. *AIAA J.*, 39(11):2033–2041, November 2001.

[5] D. J. Mavriplis. *A CFD Package for Multi-Element Airfoil High-Lift Analysis*. Scientific Simulation, Yorktown, VA, December 1996.

[6] S. Painchaud-Ouellet. Optimisation aérodynamique de profils d'aile 2d. Master's thesis, Département génie mécanique, école polytechnique de Montréal, 2003.

[7] S. Painchaud-Ouellet, C. Tribes, and J.-Y. Trépanier. Airfoil shape optimization using Navier-Stokes flow solver and NURBS representation. In *Proceedings of the 49th Annual CASI Conference*, Montréal, Québec, 2003. Canadian Aeronautics and Space Institute.

[8] L. Piegl and W. Tiller. *The NURBS Book*. Springer-Verlag, 1995.

[9] P. Spelluci. An SQP method for general nonlinear programs using only equality constrained subproblems. *Math. Prog.*, 82:413–448, 1998.

[10] S. Takahashi, S. Obayashi, and K. Nakahashi. Inverse design optimization of transonic wings based on multi-objective genetic algorithms. *AIAA J.*, 37(12):1656–1662, December 1999.

[11] C. Tribes and J.-Y. Trépanier. Airfoil shape optimization. In *CSME-MDE, International Conference on Multidisciplinary Design in Engineering*, Montréal, QC, Canada, 2001.

[12] G. N. Vanderplaats. *Numerical Optimization Techniques for Engineering Design*. Vanderplaats Research & Development, Inc., 1999.